



**HAL**  
open science

# Ultrasonic transmission through small tubes such as rat tibias for axial Young's modulus estimation: Discussion and recommendations

Didier Laux, Eric Rondet, Joel Grabulos, Rémi Dore, Léa Ollier, Anne Virsolvy, Denis Mariano-Goulart, Laurent Maïmoun

## ► To cite this version:

Didier Laux, Eric Rondet, Joel Grabulos, Rémi Dore, Léa Ollier, et al.. Ultrasonic transmission through small tubes such as rat tibias for axial Young's modulus estimation: Discussion and recommendations. *Applied Acoustics*, 2022, 188, pp.108573. 10.1016/j.apacoust.2021.108573 . hal-03495199

**HAL Id: hal-03495199**

**<https://hal.science/hal-03495199>**

Submitted on 2 Jun 2023

**HAL** is a multi-disciplinary open access archive for the deposit and dissemination of scientific research documents, whether they are published or not. The documents may come from teaching and research institutions in France or abroad, or from public or private research centers.

L'archive ouverte pluridisciplinaire **HAL**, est destinée au dépôt et à la diffusion de documents scientifiques de niveau recherche, publiés ou non, émanant des établissements d'enseignement et de recherche français ou étrangers, des laboratoires publics ou privés.

# Ultrasonic transmission through small tubes such as rat tibias for axial Young's modulus estimation: Discussion and recommendations

Didier Laux <sup>a,b</sup>, Eric Rondet <sup>c</sup>, Joel Grabulos <sup>c</sup>, Rémi Dore <sup>a,b</sup>, Léa Ollier <sup>c</sup>, Anne Virsolvy <sup>d</sup>,  
Denis Mariano-Goulart <sup>e</sup>, Laurent Maimoun <sup>e</sup>

<sup>a</sup> Université de Montpellier, IES, UMR 5214, F-34000 Montpellier, France <sup>b</sup>

CNRS, IES, UMR 5214, F-34000 Montpellier, France

<sup>c</sup> QualiSud, Université de Montpellier, Avignon Université, CIRAD, Institut Agro, IRD, Université de la Réunion, Montpellier, France <sup>d</sup>

Université de Montpellier. PhyMedExp. INSERM U1046. CNRS UMR 9214, France <sup>e</sup> Université de Montpellier. Service de Médecine Nucléaire, PhyMedExp. INSERM U1046. CNRS UMR 9214, France

**Abstract :** In the framework of in vitro osteoporosis investigation with ultrasound on rat model, we propose a study of axisymmetric modes guided in small cylindrical structures such as rat tibias. The main objective is to analyze how an ultrasonic pulse (with a frequency close to the MHz) transmitted through the cortical bone diaphysis can be used to obtain a rapid estimation of the axial Young's modulus. Thanks to a numerical approach and experimentations on bone phantoms we show that the velocity of the first arrival signal ( $V_{FAS}$ ) measured with a simple time of flight method corresponds to the maximum of the group velocity of the axisymmetric  $L_{00}$ ;  $2P$  mode. Considering the geometry of the cylinders analyzed, we show that it is possible to use this velocity to estimate the axial Young's modulus. The ratio (internal radius / thickness) is an important parameter for small tubes such as rat tibias and has to be considered for results analysis. In this framework, mCT measurements are of first interest. At the end of this communication, preliminary experiments on rat tibias are presented and discussed.

**Keywords :** Ultrasound Young's modulus, Guided modes, Rat tibias, Porosity, Osteoporosis mCT

Accepted in J Applied acoustics 2022

## 1. Introduction

Many clinical studies using ultrasound devices to explore bone tissue characteristics and to determine osteoporosis in bone have been published and a global review can be found in Laugier et al. book [1]. In various clinical situations inducing bone characteristic variations such as age-related change [2], intense training [3] and anorexia nervosa [4], broadband ultrasonic attenuation (BUA in dB.MHz<sup>1</sup>) is the parameter mostly measured with ultrasonic pulse transmission through the heel in calcaneum [4]. As mentioned in Laugier et al. [1], if the bone thickness is also measured, the normalized BUA (n-BUA) can be used. Correlations between BUA or n-BUA, bone porosity, bone mineral density (BMD) can then be established to provide means of diagnosis [4,5]. Concerning the ultrasonic velocity, measurement in tubular bones such as femur or tibia, in order to evaluate the elastic parameters of cortical bone (Young's modulus in particular), the problem appeared more complex due to the geometry of bone. Furthermore, as mentioned in Laugier et al. [1], the methods used by different authors are not detailed enough making difficult the comparison between results. So, more work has to be done to elucidate this problem. When the bones are large enough (i.e., in human or in bovine), in vitro studies are often done on bone cubes machined in various anatomical directions [6]. Thanks to measurements using longitudinal or transverse waves, the elastic moduli in the various directions can then be evaluated. Some authors have also used original vibratory methods on cubes or on whole bones [7]. Recently, Peralta et al. [8] used Resonant Ultrasonic Spectroscopy (RUS) method and obtained very good results for Young's modulus or ultrasonic velocities on human bone femurs and tibias. At last, we can also cite the axial transmission method [1]: in this approach, an ultrasonic wave propagating in the cortical bone is excited along diaphysis and received with at least 2 transducers positioned perpendicularly to diaphysis. This method does not need a complex preparation of the bone sample. Furthermore, if the frequency is high enough (MHz for human bone) so that thickness wavelength, the skimming wave (longitudinal surface wave generated for a specific critical angle of incidence) can be excited leading to a direct estimation of the

longitudinal velocity [1,9]. Furthermore, this method is applicable in vivo on human tibia or radius for instance [10].

For small animals such as rats, to our knowledge, relatively few studies have been carried out especially on tibias. Indeed, their diameter and thickness are very small and the application of the previous approaches is not easy. For instance, axial transmission should need very high frequencies which is tricky because of ultrasonic attenuation.

For works on rat femur, one can refer to the investigations of Kohles et al. [11], Han et al. [12], and Vanleene et al. [13] with transmitted longitudinal waves in axial or radial direction. For instance, Vanleene et al. [13] worked at 100 kHz on bones having cross sections ranging from 2 to 5 mm. When the authors have simply used the transmission of an ultrasonic pulse along the diaphysis and thanks to the measurement of its travel time they have deduced the velocity of the first arrival signal ( $V_{FAS}$ ). For nondispersive systems,  $V_{FAS}$  is equal to group and phase velocity. For instance, for an homogeneous sample with large dimensions compared to the wavelength,  $V_{FAS}$  corresponds to the bulk longitudinal velocity (if longitudinal transducers are used). For dispersive systems,  $V_{FAS}$  is only the velocity measured and the challenge is to link this velocity to elastic parameters of the sample. Consequently, as bone is a tubular and dispersive system, the link between elastic modulus and  $V_{FAS}$  is not trivial. The well-known relationship  $E \text{ Young's modulus} \propto \rho V_{FAS}^2$  where  $\rho$  is the bone mass density is not applicable except if the frequency tends towards 0. In this case dispersion disappears,  $V_{FAS}$  is equal to group velocity and phase velocity. Then,  $V_{FAS}$  is called bar velocity. But, when frequency increases, high dispersion appears and ultrasonic velocity decreases a lot. So, estimating Young's modulus simply with  $V_{FAS}$  becomes impossible because the relationship  $E \propto \rho V_{FAS}^2$  becomes wrong. Surprisingly, in literature, the previous simple relationship is often used, even if the frequency does not tend to zero. To justify these calculations some authors often quote the founding works of Hashmann [14] in which samples were small cubes and not small tubes. Concerning comments on  $V_{FAS}$ , phase and group velocity, one can refer to [15,16] in the case of human samples. Even if the measurement of dispersion curves has been widely

investigated, research is going on, in order to obtain a higher accuracy using specific signal processing in plates or bones [17,18].

Our study, which focuses on rat tibias, aims to identify what is exactly measured in terms of  $V_{FAS}$  with a simple transmission of an ultrasonic pulse in a rat tibia diaphysis and to analyze if evaluating the axial Young's modulus with the relationship  $E \propto qV_{FAS}^2$  relation remains possible. After a short theoretical part concerning the nature of longitudinal axisymmetric modes in infinite tubes, we will present the numerical approaches using on the one hand a commercial software (Disperse) to calculate dispersion curves and on the other hand a Finite Element (FE) calculation code. In order to validate finite elements code, dispersion curves obtained with Disperse will be compared to those deduced with ultrasonic signals simulated with finite elements. Then, we will analyze the simulated signals transmitted in a tube and the velocity ( $V_{FAS}$ ) deduced from time of flight, to identify the nature of the measured velocity. In a second step we will present the samples: phantoms and rats tibias. Then, the methods used to measure the density of rat tibias, their morphology and  $V_{FAS}$  through diaphysis will be detailed. Finally, first results obtained in terms of Young's modulus on seven rat tibias will be presented and discussed.

## 2. Theoretical background: Some basics

If one is only interested with axisymmetric modes for which the strain does not depend on the  $\theta$  angle of the cylindrical coordinates, for an infinite hollow tube, in very low frequency range, one finds the elongation or bar mode named  $L(0,1)$  propagating along the  $\delta z$  axis of the tube without radial deformation. As already mentioned, if frequency tends to zero, this mode is nondispersive and the relationship  $E \propto qV_{FAS}^2$  is applicable. However, this mode becomes highly dispersive as soon as the frequency increases. For rat tibias, it would be necessary to work with very low frequencies (<100 kHz). Working in very low frequency range is tricky because sensors diameter is very large compared to bones cross sections. For higher frequencies many dispersive modes appear and generally strongly radially deform the walls of the tube. Among these modes, the  $L(0,2)$  mode, meanwhile, has a particularity. When the product (frequency (MHz) thickness (mm)) is between 0.5 and 1.5 MHz.mm it becomes less dispersive [19,20]. For rat tibias, thickness classically ranges from 300 to 1000 mm and the product (frequency (MHz) thickness (mm)) should be close to 1 MHz.mm for frequencies around the MHz. This is the reason why we will focus our attention on this mode with MHz ultrasonic transducers.

Typical dispersion curves concerning phase and group velocities of  $L(0,1)$  and  $L(0,2)$  modes are presented in Fig. 1. They have been obtained with Disperse software and for characteristics corresponding to rat bone samples (see part 4).

## 3. Materials and methods

### 3.1. Phantom and bone samples

In order to validate the method, we used brass tubes (thickness  $e \approx 500\mu m$  and internal radius  $R_i \approx 500\mu m$ ) and a glass tube ( $e \approx 800\mu m$  and  $R_i \approx 5300\mu m$ ). For our experiments, seven tibias ( $T_0$  to  $T_6$ ) were collected after sacrifice on rats previously used in a preclinical study. All animal experimentation procedures were conformed to the Directive 2010/63/EU that was adopted on the September 22, 2010 for the protection of animals used for scientific purposes (agreement number : A34-172-38) and was approved by the Comité d'éthique en expérimentation animale LanguedocRoussillon (CEEA-LR, C2EA-36) (protocol number: APAFIS#39222016020317052023v2).

A standardized procedure was used to prepare samples. Following harvesting, the bone samples were cleaned of soft tissue excess. Their metaphysis and epiphysis were cut and the residual internal trabecular bone was

washed from the medullary cavity. The obtained samples consist in pseudo cylindrical tubes of approximately 1 cm high. The wall of these cylinders consists in the cortical bone whose properties will be studied in the following parts.

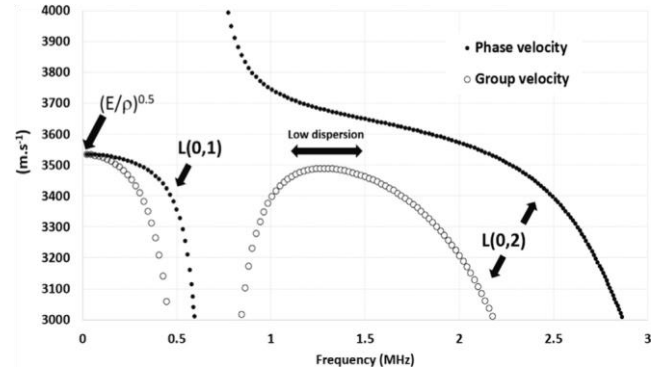


Fig. 1. Typical dispersion curves for  $L(0,1)$  and  $L(0,2)$  modes in terms of phase and group velocities in an infinite tube.

## 3.2. Simulations

### 3.2.1. Disperse software

With Disperse calculation code [21], if the mechanical properties of the material and its geometry (plate, tube, cylinder) are known, it is possible to calculate the dispersion curves. Thus, the phase velocity and the group velocity are obtained as a function of the frequency. Sample deformations during ultrasonic wave propagation can also be visualized. It is also possible to plot the ultrasonic signal after a given propagation distance. But, with Disperse it is not possible to simulate propagation in finite tubes or in more complex geometries: for instance, cylinders with thickness variations along  $\delta z$  axis. This is the reason why we have also used a Finite Element (FE) method to deduce the dispersion curves directly from the echograms.

### 3.2.2. Finite elements calculations

FE simulations were carried out with the education and research version of CAST3M software developed by the CEA in France. Simulation was performed in 2D-Axisymmetric configuration using eight-nodes squares. Convergence tests showed that it was necessary to take 10 finite elements per wavelength, which is generally the accepted standard for non-spectral finite elements. A short sinusoidal excitation with 1 period at 1 MHz was imposed in the axial direction  $\delta z$  on the top of the meshed tube. With the "dynamic" procedure, the  $\delta u_z$  displacement after a given distance and propagation time was plotted, thus forming the echogram. In rat tibias, we will see further that only the first transmitted signal is visible. In order to simulate such a case, echograms for various tube lengths were calculated. The envelope of the first transmitted signal (obtained with a Hilbert transform) was then calculated for each propagation distance.

The plot of the position of the maximum of the envelope as a function of the propagation distance led to the calculation of  $V_{FAS}$  through the diaphysis. In a second step, for the simulation we have used various echoes after several round trips in the tube. The FFT (Fast Fourier Transform) modulus was calculated.

Let us first consider the case of a non-dispersive system: it is possible to show that the FFT modulus is constituted of several peaks, regularly spaced. The difference of frequency  $\delta f$  between two peaks is constant and can be used to calculate  $V_{FAS}$  [22]. As there is no dispersion:  $V_{FAS} = \text{group velocity} = \text{phase velocity}$ . Let's now consider a tube which is a dispersive system: the distance  $\delta f$  between 2 peaks depends on the frequency. However, as each peak in the FFT corresponds to a resonance of the system it is possible to show

that the group velocity  $V_g$  at the frequency  $f_i$  can be calculated in this way (relationship (1)), where  $L$  is the tube length:

$$V_g(f_i) = L \cdot (f_{i+1} - f_{i-1}) \quad (1)$$

Thus, by locating the positions of the peaks, the group velocity as a function of the frequency can be estimated. A summary of the procedure is given in Fig. 2.

**Remark.** In simulations there is no damping. Consequently, spectra exploitation is quite easy. But on an experimental point of view, to apply the signal processing it is necessary to have at least two echoes. That is the reason why on real bone samples it does not work. Indeed, only one transmitted signal is observed and only  $V_{FAS}$  can be measured. For experiments on glass or metal tubes a compromise has to be found between damping and length. Indeed, because of duality between time and frequency if length is small, damping is small and a lot of round trips are observed. But in this case,  $(\Delta f)$  is large and only a few points are acquired on dispersion curve. On the other hand, if tubes are long,  $(\Delta f)$  is small, many points are acquired on dispersion curve but a higher damping occurs. For our experiments typical lengths around 5 cm have been used because they led to good spectra. Temporal signal and associated spectrum will be presented in part 4.2.

### 3.3. X-Ray microtomography : mCT

mCT was used to obtain bones geometric and morphometric data. This is fundamental for dispersion curves interpretation and for porosity estimation. The bone samples were scanned in the SkyScan 1272 X-rays microtomograph (Bruker mCT, Kontich, Belgium) at a nominal resolution of 5.5 mm employing an aluminum filter 0.5 mm thick, an applied x-ray tube voltage of 66 kV and a source current of 151 mA. Camera pixel binning of 2 2 was applied. The scan orbit was 180 degrees with a rotation step of 0.6 degrees. Reconstruction was carried out with a modified Feldkamp algorithm [23] using the SkyScan™ NRecon software accelerated by GPU [24]. Gaussian smoothing, ring artefact reduction and beam hardening correction were applied. Volume of interest (VOI) selections, segmentations to binary and morphometric analysis of the seven samples were all performed using SkyScan CT-Analyser (“CTAn”) software. The cortical VOI commenced about 0.35 mm (64 image slices) from the bottom of the bone sample level and extended from this position for a further 6.6 mm (1200 image slices) in a diaphyseal direction. The same global thresholds were selected for the seven samples by visual matching with greyscale images. The signal to noise ratios of the reconstructed images and segmented binary images did not necessitated any subsequent image processing. 3D morphometric parameters were calculated for cortical selected VOIs. Morphometric parameters in 3D (open, closed and total porosity, bone

volume/total volume, object volume, structure thickness...) were based on analysis of a Marching Cubes [25] type model with a rendered surface. Structure thickness and structure separation in 3D was calculated using the local thickness or “sphere-fitting” (double distance transform) method [26,27]. Surface-rendered 3D models were constructed for 3D viewing cortical analyzed regions, using SkyScan CTVolume (“CTVox”) software. Model construction was by the “Double time cubes” method [28], a modification of the Marching cubes method [25].

### 3.4. Mass density

The solid true mass density  $\rho$ (Kg/m<sup>3</sup>) of dried (105 degreesC – 24 h) and finely grinded bone samples was measured by helium pycnometry using a helium Multivolume Pycnometer 1305 micromeritics (Quantachrome Instruments, Odelzhausen, Germany). Analysis were performed in triplicate.

### 3.5. Ultrasonic experiments

Ultrasonic Olympus longitudinal transducers (central frequency 2.25 MHz) were excited with an Olympus 5073PR pulse generator. The ultrasonic signals were visualised on a Lecroy Wavejet 334 before acquisition on a personal computer via an USB-GPIB connection. All acquisitions and signal processing tasks were carried out using in-house Labview software. For brass and glass tubes, we worked in reflection configuration with one transducer because many round trips were observed. The tube was simply settled vertically on the transducer and coupled to the ultrasonic probe with a thin layer (a few mm) of honey. After ultrasonic signal acquisition, we used the signal processing presented in simulation: the FFT was performed and dispersions curves were calculated. We used various glass and brass samples having different lengths in order to also evaluate  $V_{FAS}$ . For bone samples, we worked in transmission configuration with two transducers positioned at each end of the bone because only the first transmitted signal could be observed. If  $(z)$  represents the third coordinate of cylindrical system used to describe bones, the probes are parallel to  $(z)$  and so the piezo element is perpendicular to  $(z)$ . This configuration ensures and excitation of L modes along diaphysis. After each experiment for a given length, the length was mechanically reduced with a small saw in order to perform measurements for various lengths. Here again we used the signal processing presented in simulation: after signal positions estimation (with the envelop), we plotted the arrival time versus length in order to calculate  $V_{FAS}$ .

## 4. Results

### 4.1. Simulations

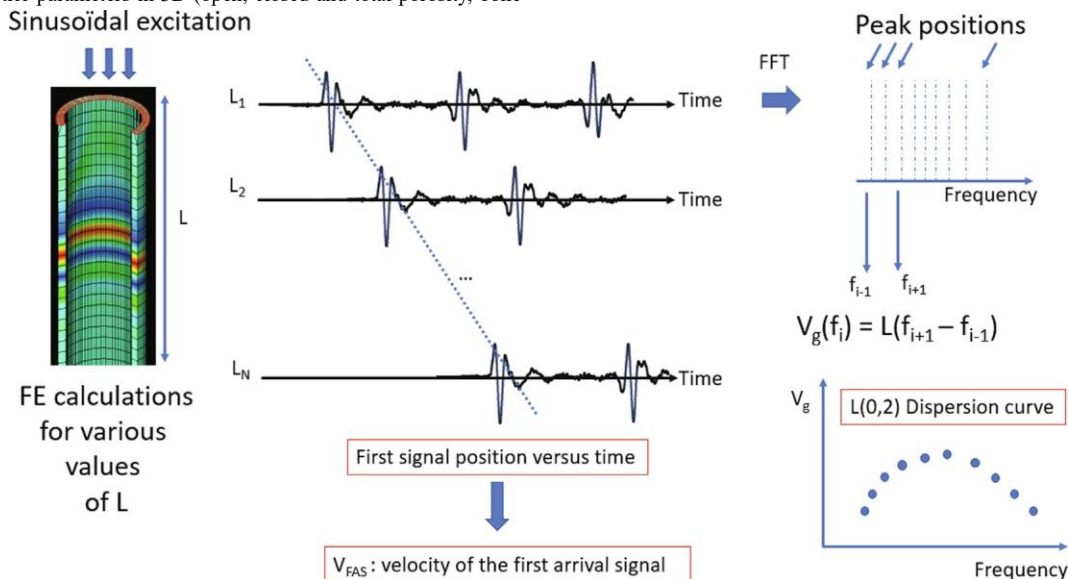


Fig. 2. Finite elements simulation and signal processing.

In order to validate our FE calculation method and the associated signal processing, a first simulation was performed on brass with the following parameters: thickness:  $e = 500\mu\text{m}$  internal

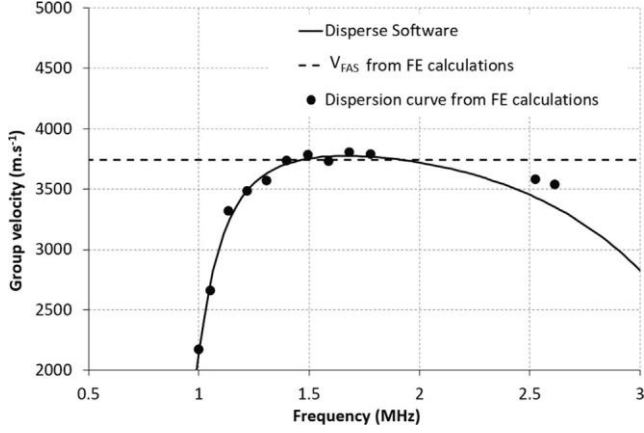


Fig. 3. Comparison between FE and Disperse simulations. Brass.  $R_i/e = 1$ .

radius:  $R_i = 500\mu\text{m}$ , mass density:  $\rho = 8500\text{ kg/m}^3$ , Young's modulus:  $E = 1265\text{ GPa}$ , Poisson's ratio:  $\nu = 0.29$ ). From FE calculations,  $V_g(f)$  (with a length  $L$  equal to 2 cm) and  $V_{FAS}$  (with  $L = 1, 2, 3$  and 4 cm) were deduced. They are compared with the result given by Disperse software in Fig. 3.

A second simulation was performed with data representing mean values for rat bone. We chose :  $e = 600\mu\text{m}$ ,  $R_i = 600\mu\text{m}$ ,  $\rho = 2000\text{ Kg/m}^3$ ,  $E = 25\text{ GPa}$ , Poisson's ratio  $\nu = 0.25$ . Here again, from FE calculations  $V_g(f)$  (with a length  $L$  equal to 2 cm) and  $V_{FAS}$  (with  $L = 1, 2, 3$  and 4 cm) were deduced.

They are compared with the result given by Disperse software in Fig. 4.

On these graphs one can notice that the maximum of the group velocity ( $V_{gMAX}$ ) is close to  $V_{FAS}$ . In fact, such an element is not very surprising because the maximum of the group velocity corresponds to the frequency for which the displacement in ( $z$ ) direction is the most homogeneous through the tube wall. This element has been checked with Disperse software: at this specific frequency, the amplitude of the ultrasonic signal reaches a maximum. So, the  $\delta u_z$  displacement (plotted with FE or measured with our ultrasonic longitudinal transducers) will be emphasized. Consequently, when  $V_{FAS}$  is calculated in temporal domain, the velocity obtained is a group velocity near this frequency where  $V_g$  reaches its maximum. In order to confirm this fact, several simulations have been made for bone, glass and brass with  $R_i/e$  ratios ranging from 1 to  $\sim 7$  (See Fig. 5). The value of  $V_{gMAX}$  depends on mechanical properties of the material and on the ( $R_i/e$ ) ratios. Simulations have also

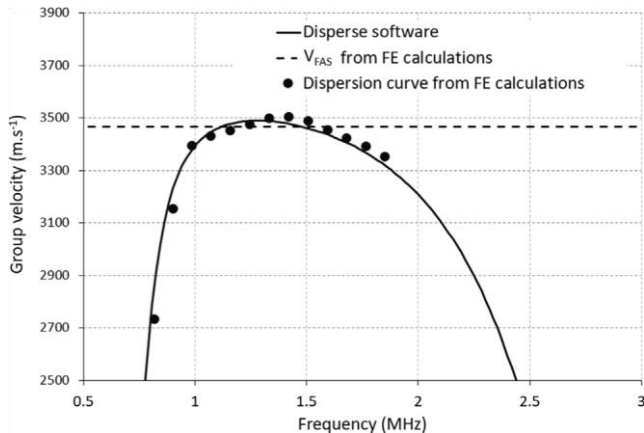


Fig. 4. Comparison between FE and disperse simulations. Bone.  $R_i/e = 1$ .

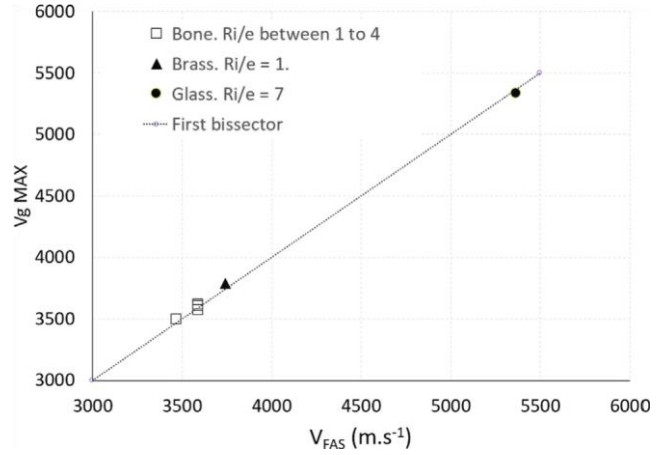


Fig 5.  $V_{gMAX}$  versus  $V_{FAS}$  for various samples and  $\frac{R_i}{e}$  ratios.

shown that for a given thickness, if  $R_i/e$  increases, the dispersions curves are displaced to the left,  $V_{gMAX}$  increases, and the plateau where the dispersion is small is larger. For a given  $R_i$ , if  $R_i/e$  increases, the dispersion curves are displaced to the right, the velocity increases and the plateau where the dispersion is small is larger. In all of these simulations we observed:

$$V_{gMAX} \sim V_{FAS} \quad (2)$$

Now, to link  $V_{FAS}$  to Young's modulus it is necessary to compare  $V_{FAS}$  to  $L(0; 1)$  group velocity: if the frequency tends to 0, we recall that the elastic modulus is directly linked to the elongation velocity  $V_{Elong}$  which represents the velocity of the  $L(0;1)$  mode with the well-known relationship  $E = \rho V_{Elong}^2$ . In our experiments,  $V_{Elong}$  is not measured. So, we propose to suppose  $E = \rho V_{FAS}^2$  and to estimate the error made regarding the values of ( $R_i/e$ ) and Poisson's ratios for a given Young modulus having a classical order of magnitude for rat bones. The results are presented in Table 1.

Regarding these results, the relationship  $E \sim \rho V_{FAS}^2$  leads to an estimation of the Young's modulus with an accuracy around 2 % when  $R_i/e \sim 2$ . We will see further that this value is a mean one for all the bones analysed. Then for a given ( $R_i/e$ ) equal to 2 (typical value for rat tibias) and a Poisson's ratio ranging between 0 and 0.3 the accuracy has also been evaluated. If Poisson's ratio tends to zero,  $E \sim \rho V_{FAS}^2$  becomes exact because the mode becomes elongational. When the Poisson's ratio is around 0.3 (value classically observed for bones), the accuracy is around 1.6 %. At last we have simulated more complex geometries (see Fig. 6) and here again the relationship  $E \sim \rho V_{FAS}^2$  remains valid. As a conclusion of this simulation part, for bones, if we apply the relationship  $E \sim \rho V_{FAS}^2$  on rat tibias for which (see part 4.3) ( $R_i/e$ ) is around 1.7 and assuming a Poisson ratio less than 0.3, the maximum error on  $E$  should be inferior to 2.5 %. So, for small tubes the relationship (3) will be used in the next parts on this paper:

$$E \sim \rho V_{FAS}^2 \quad (3)$$

#### 4.2. Experimental results on brass and glass tubes

On brass we used tubes already presented in part 3.1.  $V_{FAS}$  measurements were performed with  $L$  ranging from 1 to 4 cm. For dispersion curve evaluation, we used the 4 cm tube. Indeed, longer is the tube, smaller is the  $Df$  value between to peaks in the FFT. Consequently, more points are acquired for the dispersion curve evaluation.

Experimental signal in time domain showing echoes and spectrum used to evaluate dispersion curve are presented in Fig. 7.

Our experimental dispersion curve was then adjusted with Disperse software with the following mechanical parameters:  $E = 119.6$  GPa, Poisson's ratio = 0.296 and  $\rho = 8500 \text{Kg/m}^3$ .

Such values are in line with data from literature and depends on brass chemical composition :  $E$  between 100 and 130 GPa, Poisson's ratio between 0.28 and 0.37.5 and  $\rho$  between 7200 and 8800  $\text{Kg/m}^3$ . Regarding Fig. 8, it is obvious that  $V_{gMAX} \sim V_{FAS}$ . Using the relationship (3), the Young modulus estimated with  $V_{FAS}$  was 116 GPa. Compared to  $E$  obtained with Disperse, the difference is 3 %.

Same experiments conducted on the glass tube lead also to a good adjustment with Disperse software with:  $E = 70,5$  GPa, Poisson's ratio = 0.226 and  $\rho = 2500 \text{Kg/m}^3$ . Such values are also in line with literature. Using the relationship (3) the Young modulus estimated with  $V_{FAS}$  was 73.4 GPa. The difference reaches 4.28 %. It is higher because  $(R_i/e)$  reaches the value of 7.

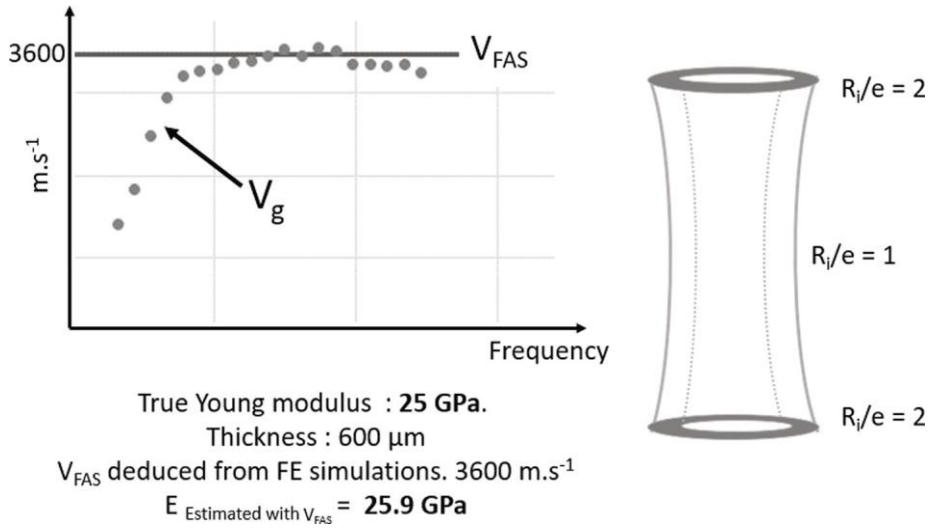


Fig. 6. FE simulations for a more complex geometry of rat tibia.  $L = 4$  cm.

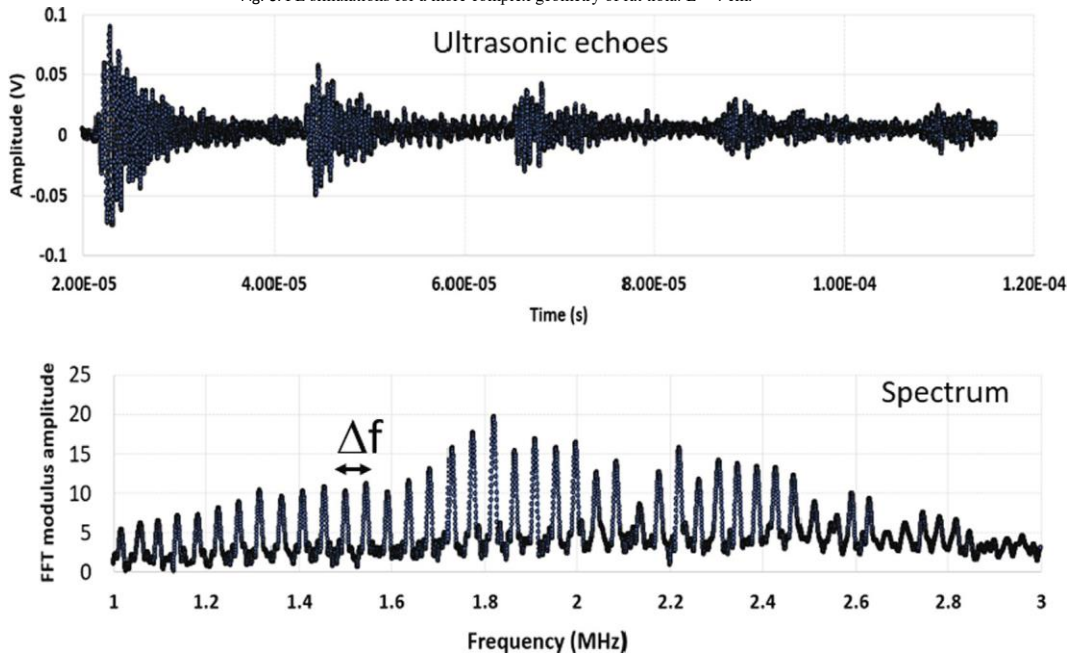


Fig. 7. Experimental signals acquired on brass sample.

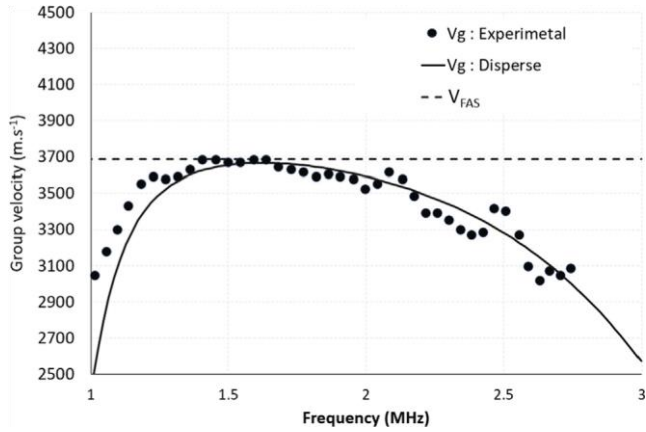


Fig. 8. Experimental results on brass.

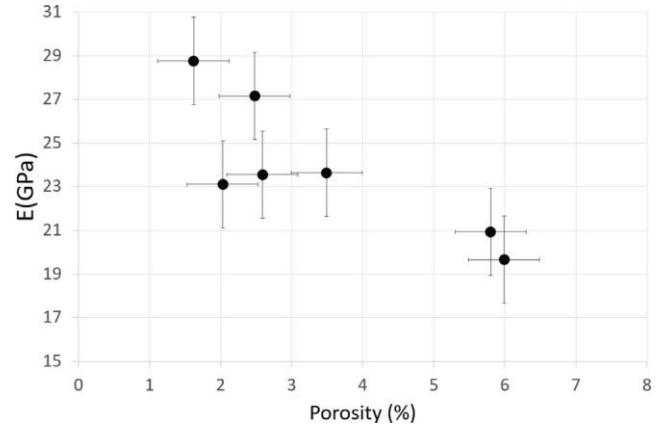


Fig. 9. Young modulus versus porosity on 7 rat tibias.

Table 1

Error between Young's modulus calculated with  $V_{FAS}$  and true Young modulus used for finite elements simulations. Finite elements parameters: Poisson's ratio  $\nu=0.25$ ,  $E=25\text{GPa}$ , mass density  $\rho=2000\text{Kg/m}^3$ .

$R_i/e$	$V_{FAS}$ (m.s <sup>-1</sup> )	$q_{V_{FAS}2}$ (GPa)	Error (%)
1	3485	24.3	2.83 1.85
2	3568	25.46	
3	3596	25.86	3.45
4	3611	26.07	4.31

Table 2

Experimental results obtained on 7 rat tibias.

Tibia	$e$ (mm)	$R_i$ (mm)	$\delta R_i/e$	P (%) $\pm 0.5$	$q$ (Kg.m <sup>3</sup> ) $\pm 130$	$V_{FAS}$ (m.s <sup>-1</sup> ) $\pm 50$	E (GPa) $\pm 2$
T0	0.68	1.43	2.1	1.62	2184	3629	29
T1	0.78	1.24	1.59	2.03	2175	3260	23
T2	0.45	0.9	2	5.8	2091	3164	21
T3	0.33	1.41	4.27	5.99	2073	3069	20
T4	0.74	1.06	1.43	2.59	1730	3300	19
T5	0.73	1.17	1.6	2.48	2110	3541	27
T6	0.81	1.27	1.57	3.49	2143	3322	21

#### 4.3. Experimental results on bone

In the following table (Table 2.) we have reported all the characteristics of tibias analysed in term of porosity measured with mCT. Thanks to the experiment performed with the Pycnometer a mean true density has been evaluated to  $2220 \pm 120 \text{ kg/m}^3$ . Then the mass density has been calculated with  $\rho_{mCT} = 2200 \cdot (1 - P_{mCT})$  where  $P_{mCT}$  is the total porosity measured in the bone sample. For  $T_2$  tibia,  $P_{mCT}$  was not obtained correctly. So, the mass density has been measured with a weighting method and porosity was then calculated. We have also reported the values of  $R_i$ ,  $e$  and  $R_i/e$  ratio. In the two last columns, the values of  $V_{FAS}$ , and  $E$  calculated with relationship (3) are reported. Considering the accuracy on  $V_{FAS}$  and density evaluation, the global accuracy on  $E$  has been estimated to  $\pm 2$  GPa. In our experiments all bones except  $T_3$  have got  $R_i/e$  ratios between 1.5 and 2. If we refer to Table 1. this means that the influence of geometry on  $E$  estimation is around 2% i.e.  $< 0.5$  GPa.  $T_3$  presents a high ( $R_i/e$ ) 4. So, for this bone, Young modulus is certainly overestimated (1 GPa). But on the other hand, the value measured is smaller and comparable to Young modulus obtained for  $T_2$ ,  $T_4$  and  $T_6$ . So, for this sample, Young modulus is clearly inferior and geometrical effects do not introduce a large bias on data interpretation. Generally speaking, if for a given experiment, variations observed on Young modulus are small it is important to check if such a variation is not simply due to a geometrical effect and not to mechanical properties

As we had only of few numbers of samples, our goal is not to give reliable behaviour laws. Indeed, in biological domain only statistical analysis have a meaning. We just want to check if the global trend observed is in line with literature. Furthermore, it will give new data on rat tibias for which a very few data are available in literature (See Fig. 9). The slope for  $E$  modulus versus porosity is 1.5. Literature data from Vanleene et al. [13] on femurs lead to a slope of 2. The values of Young moduli reported in this communication were in the same order of magnitude compared to our data. Nevertheless, the values are a little bit inferior. If we refer to [29], this is perhaps due to the fact that our measurements were performed on dry bone samples. Furthermore, regarding literature it seems that Young modulus for femurs is smaller compared to tibias

[30].

#### 5. Conclusion and recommendations

In this paper we have shown that the  $L(0;2)$  mode can be used for rat tibias ultrasonic investigations for frequencies close to the MHz. Using longitudinal transducers, the velocity of the first arrival signal measured in time domain by a simple time-of-flight method corresponds in fact to the maximum of the group velocity of the  $L(0; 2)$  mode. Moreover, the favorable geometry of the rat tibias  $R_i/e \sim 2$  leads to a good estimation of the axial Young's modulus by a simple relation generally valid for infinite cylinders when frequency tends towards 0. However, in order to not introduce experimental bias due to 3D geometry bones, we recommend to explore geometric parameters with mCT. Nevertheless, in the case of this device is not available, basic geometrical mechanical analysis with caliper provide sufficient precision in the evaluation of these parameters. The first results obtained on 7 rat tibias have shown that, as expected, porosity has a strong influence on the Young's modulus. The use of this approach in the framework of preclinical studies aiming at studying the effect of treatment on osteoporosis seems to us recommended because it is simple to implement and can even be transposed in the future on commercial ultrasonic devices usually dedicated to the measurement of the BUA and the ultrasonic velocity on calcaneum.

## CRedit authorship contribution statement

Didier Laux: Funding acquisition, Conceptualization, Methodology, Investigation, Writing – original draft. Eric Rondet: Investigation, Writing – review & editing. Joel Grabulos: Investigation, Writing – review & editing. Rémi Dore: Investigation, Writing – review & editing. Léa Ollier: Investigation, Writing – review & editing. Anne Virsolvy: Resources, Writing – review & editing. Denis Mariano-Goulart: Resources, Writing – review & editing. Laurent Maimoun: Funding acquisition, Conceptualization, Methodology, Investigation, Writing – original draft.

## Declaration of Competing Interest

The authors declare that they have no known competing financial interests or personal relationships that could have appeared to influence the work reported in this paper.

## Acknowledgements

This work was supported by the LabEx NUMEV: Digital and Hardware Solutions, Environmental and Organic Life Modeling (ANR-10-LABX-0020). <https://anr.fr/ProjetIA-10-LABX-0020>

## References

- [1] Laugier P, Haïat G. Bone Quantitative Ultrasound. Springer; 2011. <https://doi.org/10.1007/978-94-007-0017-8>.
- [2] Schott AM, Hans D, Sornay-Rendu E, Delmas PD, Meunier PJ. Ultrasound measurements on os calcis: precision and age-related changes in a normal female population. *Osteoporos Int* 1993;3(5):249–54. <https://doi.org/10.1007/BF01623828>.
- [3] Maïmoun L, Coste O, Georgopoulos NA, Roupas ND, Mahadea KK, Tsouka A, et al. Despite a high prevalence of menstrual disorders, bone health is improved at a weight-bearing bone site in world-class female rhythmic gymnasts. *J Clin Endocrinol Metab* 2013;98(12):4961–9. <https://doi.org/10.1210/jc.2013-2794>.
- [4] Maïmoun L, Renard E, Huguet H, Lefebvre P, Boudousq V, Mahadea K, et al. The quantitative ultrasound method for assessing low bone mass in women with anorexia nervosa. *Arch Osteoporosis* 2021;16(1). <https://doi.org/10.1007/s11657-020-00870-w>.
- [5] Alomari AH, Al-Qahtani SM, Langton CM. In-vitro comparison of volumetric and areal bone mineral density measurements between ultrasound transit time spectroscopy and microcomputed tomography. *Appl Acoust* 2021;179:108072. <https://doi.org/10.1016/j.apacoust.2021.108072>.
- [6] Njeh CF, Hodgskinson R, Currey JD, Langton CM. Orthogonal relationships between ultrasonic velocity and material properties of bovine cancellous bone. *Med Eng Phys* 1996;18(5):373–81. [https://doi.org/10.1016/1350-4533\(95\)00064-X](https://doi.org/10.1016/1350-4533(95)00064-X).
- [7] Reem Y, Fakhreddine A, Sayegh M, Mustapha S, Hamade RF. Dynamic assessment and modeling of the modal frequencies and shapes of bovine tibia. *ASME J Nondestructive Evaluation* 2018;1(4):. <https://doi.org/10.1115/1.4040797041006>.
- [8] Peralta L, Maeztu Redin JD, Fan F, Cai X, Laugier P, Schneider J, et al. Bulk wave velocities in cortical bone reflect porosity and compression strength. *Ultrasound Med Biol* 2021;47(3):799–808. <https://doi.org/10.1016/j.ultrasmedbio.2020.11.012>.
- [9] Cheeke JDN. Fundamentals and applications of ultrasonic waves. Second edition. CRC Press; 2012.
- [10] Laugier P, Padilla F, Peyrin F, Raum K, Saïed A, Talmant M, et al. Apport des ultrasons dans l'exploration du tissu osseux. Current trends in the ultrasonic investigation of bone. *ITBM-RBM* 2005;26(5-6):299–311. <https://doi.org/10.1016/j.rbmret.2005.07.002>.
- [11] Kohles SS, Carteeff GD, Vanderby R. Cortical elasticity in aging rats with and without growth hormone treatments. *J Med Eng Technol* 1996;20(4-5):157–63. <https://doi.org/10.3109/03091909609008396>.
- [12] Han SM, Szarzanowicz TE, Ziv I. Effect of ovariectomy and calcium deficiency on the ultrasound velocity, mineral density and strength in the rat femur. *Clin Biomech* 1998;13(7):480–4. [https://doi.org/10.1016/s0268-0033\(98\)00019-9](https://doi.org/10.1016/s0268-0033(98)00019-9).
- [13] Vanleene M, Rey C, Tho HB. Relationships between density and Young's modulus with microporosity and physico-chemical properties of Wistar rat cortical bone from growth to senescence. *Med Eng Phys* 2008;30(8):1049–56. <https://doi.org/10.1016/j.medengphy.2007.12.010>.
- [14] Ashman RB, Cowin SC, Van Buskirk WC, Rice JC. A continuous wave technique for the measurement of the elastic properties of cortical bone. *J Biomech* 1984;17(5):349–61. [https://doi.org/10.1016/0021-9290\(84\)90029-0](https://doi.org/10.1016/0021-9290(84)90029-0).
- [15] Wear KA. Group velocity, phase velocity, and dispersion in human calcaneus in vivo. *J Acoust Soc Am* 2007;121(4):2431–7. <https://doi.org/10.1121/1.2697436>.
- [16] Wear KA. The dependence of time-domain speed-of-sound measurements on center frequency, bandwidth, and transit-time marker in human calcaneus in vitro. *J Acoust Soc Am* 2007;122(1):636–44.
- [17] Chen Q, Xu K, Ta D. High-resolution Lamb waves dispersion curves stimulation and elastic property inversion. *Ultrasonics* 2021;115:106427. <https://doi.org/10.1016/j.ultras.2021.106427>.
- [18] Xu K, Minonzio JG, Ta D, Hu B, Wang W, Laugier P. Sparse SVD method for high-resolution extraction of the dispersion curves of ultrasonic guided waves. *IEEE TUFFC* 2016;63(10):1514–24. <https://doi.org/10.1109/TUFFC.2016.2592688>.
- [19] Rose JL. Ultrasonic guided waves in solid media. Cambridge University Press; 2014.
- [20] Pavlakovic BN. Leaky guided ultrasonic waves in NDT. Thesis or dissertation. Imperial College London (University of London); 1998.
- [21] Disperse Software. Imperial College London. <https://www.imperial.ac.uk/nondestructive-evaluation/products-and-services/disperse/>.
- [22] Rosenkrantz E, Ferrandis JY, Augereau F, Lambert T, Fourmentel D, Tiratay X. An innovative acoustic sensor for in-pile fission gas composition measurements. *IEEE Trans Nucl Sci* 2013;60(2):1346–53. <https://doi.org/10.1109/TNS.2013.2252624>.
- [23] Feldkamp LA, Davis LC, Kress JW. Practical cone-beam algorithm. *J. Opt Soc Am* 1984;1(6):612–9. <https://doi.org/10.1364/JOSAA.1.000612>.
- [24] Yan G, Tian J, Zhu S, Dai Y, Qin C. Fast cone-beam CT image reconstruction using GPU hardware. *J X-ray Sci Technol* 2008;16(4):225–34.
- [25] Lorensen WE, Cline HE. Marching cubes: a high resolution 3d surface construction algorithm. *Comput Graph* 1987;21(4):163–9. <https://doi.org/10.1145/37401.37422>.
- [26] Borgefors G. On digital distance transforms in three dimensions. *Comput Vis Image Underst* 1996;64(3):368–76. <https://doi.org/10.1006/cviu.1996.0065>.
- [27] Remy E, Thiel E. Medial axis for chamfer distances: computing look-up tables and neighbourhoods in 2D or 3D. *Pattern Recogn Lett* 2002;23(6):649–61.
- [28] Bouvier DJ. Double-time cubes: a fast 3d surface construction algorithm for volume visualisation. *Int Conf Imaging Sci Syst Technol* 1997.
- [29] Currey JD, Landete-Castillejos T, Estevez JA, Olguin A, Garcia AJ, Gallego L. The Young's modulus and impact energy absorption of wet and dry deer cortical bone. *TOBONEJ* 2009;1(1):38–45.
- [30] Schrieffer JL, Robling AG, Warden SJ, Fournier AJ, Mason JJ, Turner CH. A comparison of mechanical properties derived from multiple skeletal sites in mice. *J Biomech* 2005;38(3):467–75. <https://doi.org/10.1016/j.jbiomech.2004.04.020>.